Journal of Materials Chemistry A

Accepted Manuscript

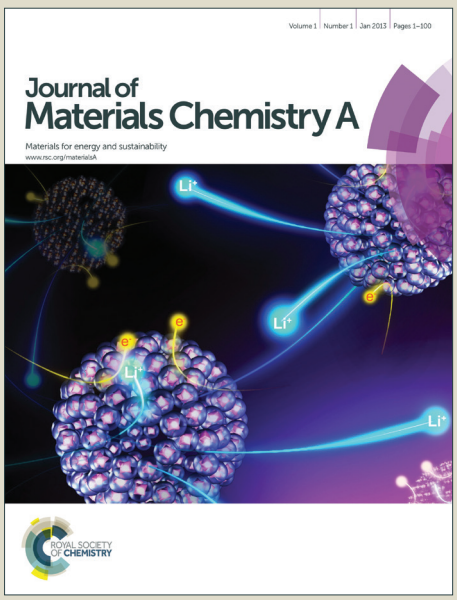

ROYAL SOCIETY OF CHEMISTRY

www.rsc.org/materialsA

Cite this: DOI: 10.1039/c0xx00000x

www.rsc.org/xxxxxx

ARTICLE TYPE

One-step preparation of ultrathin nitrogen-doped carbon nanosheets with ultrahigh pore volume for high-performance supercapacitors

Hui Peng[a], Guofu Ma*[a], Kanjun Sun[b], Jingjing Mu[a] and Ziqiang Lei*[a]

Received (in XXX, XXX) Xth XXXXXXXXX 20XX, Accepted Xth XXXXXXXXX 20XX

DOI: 10.1039/b000000x

A facile one-step activation and nitrogen-doped combination method is developed for preparation of nitrogen-doped graphene-like carbon nanosheets (N-CNSs). The N-CNSs have abundant wrinkled structures and ultrahigh pore volume (3.19 cm^3 g^{-1}) as a high-performance electrode material for supercapacitors.

Supercapacitors, a class of electrical energy storage devices with ultrahigh power density, fast charging/discharging, and exceptionally long cycling life, have attracted increasing attention owing to their widespread applications, such as hybrid electric vehicles, portable electronic equipments, uninterruptible power supplies and other devices.[1] Based on the charge-storage mechanism, supercapacitors can be divided into two categories: one is the electrical double-layer capacitors (EDLCs), where the capacitance arises from pure electrostatic charge accumulated at the electrode/electrolyte interface;[2] the other is the pseudocapacitors, where the capacitance comes from fast and reversible faradaic reactions at the electrode/electrolyte surface.[3] Transition metal oxides or hydroxides, such as RuO_2, MnO_2, $Ni(OH)_2$ etc., and conductive polymers have been used to increase specific capacitance via a variety of reversible oxidation states for highly efficient redox charge transfer.[4] However, low electrical conductivity, poor cycle stability and high price have limited the practical application of those pseudocapacitive materials.[5] In this regard, carbon materials are regarded as the most promising candidate electrode materials for electrical energy storage devices.

Two-dimensional (2D) structures (nanosheets), especially 2D porous carbon materials, are being increasingly researched for energy storage/conversion devices due to they have more active sites than 0D and 1D structures and exhibit more effective surface than other structures.[6] Moreover, the 2D porous carbon materials have some superior properties including small weight, high electrical conductivity and large surface area, which interestingly, correspond exactly to the requirement for supercapacitors.[7] More recently, the development of supercapacitors has focused on the use of 2D graphene, owing to its excellent electrical and mechanical properties, chemical stability, and high theoretical surface area.[8] Zhu research group prepared graphene woven-fabric films or multi-layer graphene and porous carbon woven composite films by chemical vapor deposition on metal mesh substrates as novel electrode materials with high performance for supercapacitors.[9] Wen et al. reported a reliable route for preparing highly crumpled nitrogen-doped graphene nanosheets (C-NGNSs) that combine the advantages of high pore volume and nitrogen doping showed excellent capacitive behavior.[10] However, more or less-severe drawbacks, such as the complex process, low yields and high cost in the preparation still preclude widespread and practical use of graphene materials in commercial supercapacitors.[11] Currently, 2D graphene-like layered structure carbon nanosheets have attracted great interest as an electrode material for supercapacitors, because of it combine the some properties of graphene and high yields in the preparation.[12] Further, the incorporation of heteroatoms (such as nitrogen or oxygen) into carbon materials seems to be the most promising method for enhancing capacity, surface wettability, and electronic conductivity of electrode materials.[13] However, Zhu et al. recently reported that the amorphous nitrogen doped carbon film possess larger ion transport resistance than graphene, which is due to the polycrystalline graphene film maintains a relatively continuous pathway for ions diffusion along the film thickness.[14] In fact, several factors significantly affect the electrochemical performances of carbon materials including electrical conductivity, specific surface area, pore size and distribution, pore volume and surface properties of electrode materials.[15] Therefore, to build high-performance supercapacitors, carbon materials should be elaborately designed by taking the morphology and hetero-atomic defects into consideration. The nitrogen doped graphene-like carbon nanosheets seems to meet these requirements and thus is attractive for supercapacitor applications.

In this paper, we developed a one-step activation and nitrogen-doped combined method using macroporous anion exchange resin (AER) as a carbon precursor, the combination of $Ca(OH)_2$ and NH_4Cl as an activator and nitrogen source to prepare novel highly crumpled nitrogen-doped graphene-like carbon nanosheets (N-CNSs). The N-CNSs have a pore volume as high as 3.19 cm^3 g^{-1} and used as an electrode material for high-performance supercapacitor. Benefiting from the highly crumpled graphene-like nanostructure and effective nitrogen doping, the N-CNSs exhibit high capacity, excellent rate capability, and extraordinary long cycle performance.

The novel N-CNSs is designed on the basis of the following: i) macroporous strongly basic quaternary ammonium-type polystyrene type AER comprises of quaternary ammonium groups ($(CH_3)_3N$-CH_2-, Fig. 1a). When the AER used as carbon precursors, it contains not only the special macropore structure,

but also can provide a nitrogen source; ii) The combination of $Ca(OH)_2$ and NH_4Cl can be used as an activator and nitrogen source, because of $Ca(OH)_2$ react with NH_4Cl to form $CaCl_2$ and NH_3 in the process of heating. Chemical activation is held in the presence of dehydrating reagents which influence pyrolytic decomposition and inhibit tar formation.[16] Similarly, the $Ca(OH)_2$ and $CaCl_2$ also has dehydration performance, which is similar to traditional activators such as KOH and $ZnCl_2$. Carbon materials with high surface areas and some porosity might be produced through the chemical activation by using these activation agents.[17] Meanwhile, nitrogen-containing functional groups can be introduced in AER-base carbon materials through reaction with the generated ammonia gas. The synthesized N-CNSs contains: i) abundant wrinkled structures and ultrahigh pore volume, which can provide a high surface area and a short diffusion distance to the interior surfaces, resulting in a high rate capability; ii) effective nitrogen doping in carbon nanosheets, which exhibits an enhanced pseudocapacitive behaviour; iii) 2D graphene-like nanosheets architecture provides excellent electrical conductivity.[18]

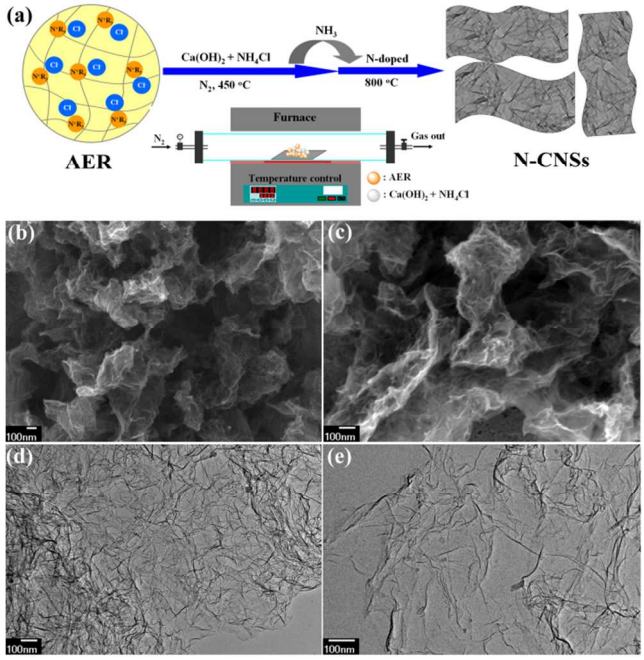

Fig. 1 (a) Schematic of the preparation process of N-CNSs; (b,c) SEM images of the N-CNSs-800; (d,e) TEM images of the N-CNSs-800.

Fig. 1a describes the entire procedure for preparing N-CNSs. In brief, the pretreated macroporous AER was mixed with $Ca(OH)_2$ and NH_4Cl placed in tube furnace. The mixtures were firstly activation and produce ammonia at 450 °C in noncurrent N_2 atmosphere. Subsequently, the graphitization and nitrogen-doped process of the carbon precursor was under a slow-flowing N_2 atmosphere by heating the sample at 700, 800 and 900 °C, respectively. Therefore, the AER could be effectively graphitization and the generated ammonia gas could completely decompose to free radicals (such as $^{+}NH_2$ and ^{+}NH) that provide nitrogen sources for finally evolving into N-CNSs. The samples were denoted as N-CNSs-700, N-CNSs-800 and N-CNSs-900, respectively. For comparison purpose, we adopt $Ca(OH)_2$ activation method without NH_4Cl to preparation of AER-base carbon materials at 800 °C, namely NC-800. In this work, N-CNSs with 2.87 wt% N obtained at 800 ºC, namely N-CNSs-800 described above, were characterized and used for supercapacitor applications unless otherwise specified.

The N-CNSs-800 displays a fluffy and distinct crumpled structure, which is revealed by typical SEM images with different magnifications (Fig. 1b-c). These crumpled graphene-like nanosheets randomly aggregate and closely associate with each other to form a disordered solid, meaning that crumpled graphene-like sheets can effectively prevent the aggregation of the sheets. In the low carbonization temperature, N-CNSs-700 shows an interconnected framework with stacking structure (Fig. S1a-b, ESI). As the carbonization temperature up to 900 °C, a large area of nanosheets with the abundant wrinkled structures is obtained (Fig. S1c-d, ESI). Moreover, the thickness of the nanosheets walls is larger than N-CNSs-800. In contrast, the NC-800 prepared by $Ca(OH)_2$ activation shows a porous structure in large lumps rather than the crumpled nanosheets (Fig. S1e-f, ESI). The interconnected crumpled structure was further confirmed by TEM (Fig. 1d-e). The N-CNSs-800 sample exhibits a folding silk-like morphology with highly interconnected crumpled and scrolling simultaneously viewed on the surface. Besides, the thickness of the graphite layers was also confirmed by high-resolution TEM (Fig. S2, ESI).

The N_2 adsorption-desorption plots of N-CNSs-800 sample (Fig. 2a) show a type IV isotherm with gradual increase positive slope in the range P/P_0=0.4-0.8, which indicates the presence of a certain amount of mesopores in this sample. A steep increase in the amount of adsorbed N_2 at relative pressures P/P_0 above 0.8 can be attributed to the N_2 adsorption in very large cavities, i.e. crumpled voids and/or macropores above 50 nm in size.[19] The specific surface area of N-CNSs-800 sample measured by the Brunauer-Emmett-Teller (BET) method is 549.5 m^2 g^{-1}. Surprisingly, the N-CNSs-800 shows an ultrahigh pore volume of 3.19 cm^3 g^{-1}, which is the higher value than in the reported ordered mesoporous carbon and most of the graphene materials to our knowledge.[20] The BET surface area and pore structure characterization parameters of N-CNSs from different carbonization temperature and NC-800 are summarized in Table S1 and Fig. S3, Supporting Information.

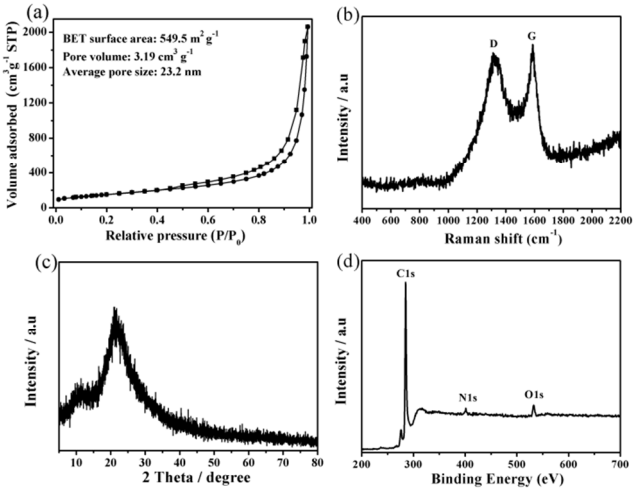

Fig. 2 (a) Nitrogen adsorption/desorption isotherms of the N-CNSs-800; (b) Raman spectrum of the N-CNSs-800; (c) X-ray diffraction pattern of

the N-CNSs-800 and (d) X-ray photoelectron spectroscopy (XPS) of N-CNSs-800.

A direct comparison between the N-CNSs and NC-800 can be revealed by the photograph of these samples (Fig. S4, ESI). The N-CNSs obvious occupy much larger bulk volume than the NC-800 at the same masses. Elemental analysis (Table 1) reveals that N content in N-CNSs-800 is 2.87 wt%, much higher than NC-800 (0.93 wt%). These results further demonstrate that the combination of $Ca(OH)_2$ and NH_4Cl is used as an activator and nitrogen source to the preparation of N-CNSs, which can significantly enhanced its pore volume and effective nitrogen doping in carbon nanosheets. The activator and the generated ammonia gas will lead to maximum volume expansion of AER and a large number of crumpled graphene-like nanosheets randomly aggregate during the annealing treatment. Therefore, it is reasonable that the high pore volume could be attributed to the gap between random aggregate of nanosheets and these crumpled voids. Fig. 2b shows the Raman spectra of the N-CNSs-800. The peak positions of the D and G bands are 1310 and 1588 cm^{-1}, respectively. The D band is a common feature of all disordered graphitic carbon, while the G band is closely related to a graphitic carbon phase with a sp^2 electronic configuration, such as graphene layers.[21] As can be seen in the spectrum, the N-CNSs-800 exhibits a strong G-band signal and a slightly lower intensity D band with a G/D intensity ratio of 1.06. These results demonstrate that the highly crumpled N-CNSs comprise turbostratic carbon with a weakly ordered graphitic microstructure. Fig. 2c shows the typical XRD patterns of the N-CNSs-800. Unusually, two broad peaks at 2θ=11.6° and 21.6° are observed in the crumpled graphene-like nanosheets. The broad (002) diffraction peak of N-CNSs-800 is centered at around 21.6°, and the corresponding interlayer spacing (0.41 nm) is larger than natural graphite (0.34 nm), which can be interpreted in terms of short-range order of the graphene sheets along the stacking direction and considerable conjugated sp^2 carbon network has been restored.[22] In addition, the weak peak at 2θ=11.6° is similar to the intertube space of multiwalled carbon nanotubes, which originates from the relatively uniform spacing of the channel at the folding axis.[23] The surface composition of N-CNSs-800 sample is further studied by XPS (Fig. 2d). There are three peaks at around 284.5, 401.5 and 532.2 eV that correspond with C1s peak of sp^2 carbon, N1s peak of the doped nitrogen and O1s spectrum, respectively. In the high resolution scan (Fig. S5, ESI), three types of N-containing groups could be verified on the surface of N-CNSs-800, including pyridinic N (N-6), pyrrolic N (N-5) and quaternary N (N-Q), corresponding to the peaks at 398.7, 400.2 and 401.7 eV, respectively, indicating that nitrogen atoms are in different binding states inserted into the graphene-like nanosheets.[24] The N-CNSs structure provides an interconnected crumpled framework including moderate surface areas and ultrahigh pore volumes associated with many porous structures from these crumpled voids. The nanosheets are loosely stacked in sample, along with the presence of nitrogen within the carbon structures, which is benefical to improve the ion-buffering reservoirs and shorten the ion diffusion channels for supercapacitor.

A three-electrode system was first used to evaluate the electrochemical properties of the N-CNSs (Fig. 3). Fig. 3a shows the cyclic voltammograms (CVs) of different electrodes at a scan rate of 50 mV s^{-1} in 6.0 M KOH aqueous solution. All the CV curves exhibit quasi-rectangular shapes indicating ideal capacitive behavior. Obviously, the N-CNSs-800 has a higher specific capacitance than other electrodes, because of the linear relation between specific capacitance and CV curve area. For N-CNSs-800, rectangular-like shapes of the CVs (Fig. 3b) are observed even at 200 mV s^{-1}. The galvanostatic charge/discharge curves of N-CNSs-800 electrodes at various current densities are shown in Fig. 3c. The corresponding specific capacitance was calculated based on galvanostatic charge/discharge method, and the correlation between the specific capacitance and the various current densities for different electrodes is presented in Fig. 3d. The N-CNSs-800 has the highest capacity among all electrodes at the same current densities. In addition, the specific capacitance of N-CNSs-800 as high as 249 F g^{-1} at a current density of 1.0 A g^{-1} and 207 F g^{-1} (about 83% capacitance retention) even at a high current density of 20 A g^{-1}. The results indicate a very fast and efficient charge transfer and the high capacitance of N-CNSs-800 electrode can be maintained under high current density. Nyquist plots of N-CNSs-800 and NC-800 in 6 M KOH is shown in Fig. S6. As seen from the expanded high frequency region of the Nyquist plots (inset in Fig. S6), N-CNSs-800 has lower charge-transfer resistance (R_{ct}) than NC-800. Therefore, it is reasonable that 2D graphene-like nanosheets architecture provides excellent electrical conductivity. We also compared the BET surface area, pore volume and capacitance values of N-CNSs with different carbon-based supercapacitors previously reported in the literatures, as listed in Table S2, Supporting Information.

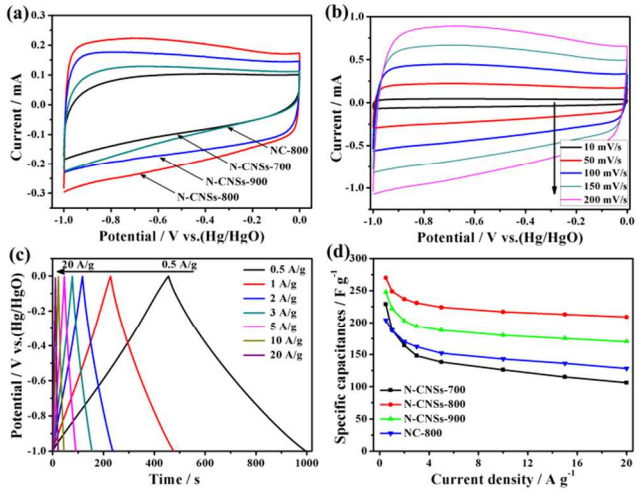

Fig. 3 (a) CVs of different electrodes at a scan rate of 50 mV s^{-1}; (b) CVs of N-CNSs-800 electrode at various scan rates; (c) Galvanostatic charge/discharge curves of N-CNSs-800 electrodes at various current densitie; (d) specific capacitance as a function of the current densities.

For practical application, we have fabricated a symmetric two-electrode cell in neutral aqueous electrolytes (0.5 M Na_2SO_4). Fig. 4a shows the CV curves of the symmetric cell at different voltage windows. Surprisingly, the stable electrochemical windows of the symmetric cell can be extended to 1.8 V. It can be concluded that the useful potential window for supercapacitor can be extended to 1.8 V without any significant distortion to the CV curve. The CV curves in Fig. 4b are quasi-rectangular shapes of the CVs with the operating voltage up to 1.8 V are observed even at 200 mV s^{-1},

indicating a very fast and efficient charge transfer. Furthermore, galvanostatic charge/discharge curves in Fig. 4c indicated the charging curves are almost symmetrical with their discharging counterpart as well as good linear voltage-time profiles, demonstrating a good capacitive performance. The N-CNSs based symmetric cell give an specific capacitance as high as 187 F g^{-1} at a current density of 0.5 A g^{-1} and 129 F g^{-1} at a current density of 10 A g^{-1} (Fig. 4d). The Ragone plot (Fig. 4e) of the supercapacitors calculated from Fig. 4c shows that the highest energy density is 20.8 Wh Kg^{-1} with a power density of 225 W Kg^{-1} and remained 13.3 Wh Kg^{-1} at 5872 W Kg^{-1}. The value surpasses most of the other reported nitrogen-doped graphene supercapacitors with an aqueous solution electrolyte (8.4 Wh kg^{-1})[25] and even comparable with boron and nitrogen co-doped monolithic graphene aerogels based solid-state supercapacitor.[26] EIS measurement of the whole cell is shown in Fig. S7. The symmetric cell has small diameter of the semicircle on the real component and a vertical line at low frequencies, which indicates that the device has excellent electrochemical performance.[27] The stability of the N-CNSs supercapacitor was also evaluated using the galvanostatic charge/discharge technique at a current density of 3 A g^{-1} (Fig. 4f). It is worth noting that the specific capacitance shows obviously increases before the initial 1000 cycles and then decreases very slowly for the subsequent cycles. The increase of the specific capacitance during the first 1000 cycles is probably due to the improved wettability of the electrode and the activation process of the electroactive material.[22] These results indicate that N-CNSs-800 has excellent electrochemical stability and a high degree of reversibility.

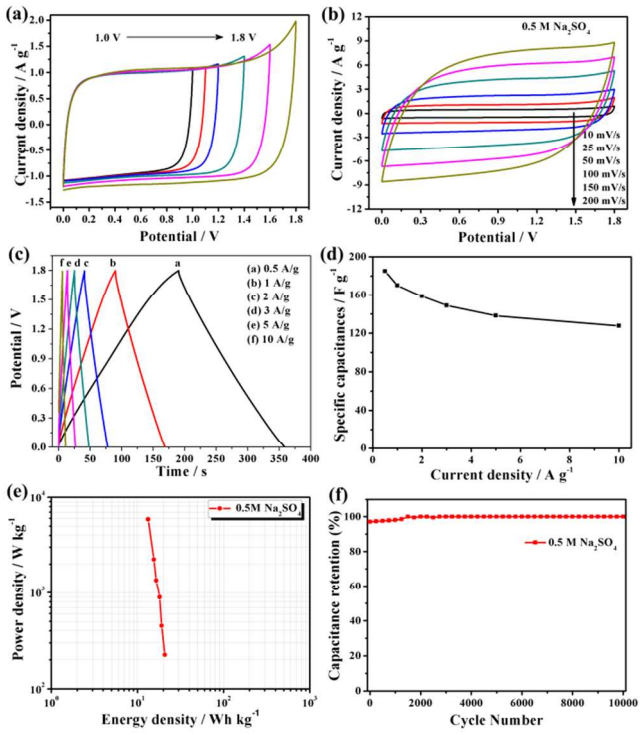

Fig. 4 (a) CV curves of the symmetric two-electrode cell at different voltage windows in 0.5 M Na_2SO_4 aqueous electrolytes; (b) CV plots of the symmetric cell at various scan rates; (c) Galvanostatic charge/discharge curves of symmetric cell at various current densitie; (d) Specific capacitance as a function of the current densities; (e) Ragone plots of the N-CNSs-800 electrode; (f) Cycling stability test at 3 A g^{-1}.

Conclusions

In conclusion, we have developed a rapid, low cost and scalable route for preparation of N-CNSs. The as-prepared N-CNSs exhibit a porous, loose, ultrahigh pore volume and highly wrinkled morphology. The unique structures endow the high-rate transportation of electrolyte ions and electrons throughout the electrode matrix, resulting in excellent electrochemical performance. Furthermore, the present approach allows for facile and scalable preparation of graphene-like nanosheets with N-doping and crumpled structures. This novel carbon material is also expected to be useful as an electrode material in other energy storage/conversion devices, as media for hydrogen storage, as catalysts for fuel cells applications.

Notes and references

[a] *Key Laboratory of Eco-Environment-Related Polymer Materials of Ministry of Education, Key Laboratory of Polymer Materials of Gansu Province, College of Chemistry and Chemical Engineering, Northwest Normal University, Lanzhou 730070, China*
Fax/Tel: +86-931-7975121;
E-mail: magf@nwnu.edu.cn; Leizq@nwnu.edu.cn
[b] *College of Chemistry and Environmental Science, Lanzhou City University, Lanzhou 730070, China*

† Electronic Supplementary Information (ESI) available: [Experimental details and electrochemical measurements. Fig. S1-S6 and Table S1-S2]. See DOI: 10.1039/b000000x/

1 G. Wang, L. Zhang, J. Zhang, *Chem. Soc. Rev.,* 2012, **41**, 797; Z. Chen, Y. Yuan, H. Zhou, X. Wang, Z. Gan, F. Wang, Y. Lu, *Adv. Mater.,* 2014, **26**, 339.
2 Y. Yun, S. Cho, J. Shim, B. Kim, S. Chang, S. J. Baek, Y. S. Huh, Y. Tak, Y. W. Park, S. Park, H. J. Jin, *Adv. Mater*., 2013, **25**, 1993.
3 L. Zhang, X. Zhao, *Chem. Soc. Rev*., 2009, **38**, 2520.
4 G. A. Snook, P. Kao, A. S. Best, *J. Power Source*s, 2011, **196**, 1.
5 J. Jiang, Y. Li, J. Liu, X. Huang, C. Yuan, X. W. D. Lou, *Adv. Mater.,* 2012, **24**, 5166; X. Lu, M. Yu, G. Wang, T. Zhai, S. Xie, Y. Ling, Y. Tong, Y. Li, *Adv. Mater*., 2013, **25**, 267; H. Peng, G. Ma, K. Sun, J. Mu, H. Wang, Z. Lei, *J. Mater. Chem. A,* 2014, **2**, 3303.
6 M. Choi, K. Na, J. Kim, Y. Sakamoto, O. Terasaki, R. Ryoo, *Nature,* 2009, **461**, 246.
7 J. Liu, X. W. Liu, *Adv. Mater.,* 2012, **24**, 4097.
8 M. Pumera, *Chem. Soc. Rev.,* 2010, **39**, 4146; T. Y. Kim, G. Jung, S. Yoo, K. S. Suh, R. S. Ruoff, *ACS Nano,* 2013, **7**, 6899; H. Jiang, P. S. Lee, C. Li, *Energy Environ. Sci.,* 2013, **6**, 41.
9 X. Li, X. Zang, Z. Li, X. Li, P. Li, P. Sun, X. Lee, R. Zhang, Z. Huang, K. Wang, D. Wu, F. Kang, H. Zhu, *Adv. Funct. Mater.* 2013, **23**, 4862; X. Zang, Q. Chen, P. Li, Y. He, X. Li, M. Zhu, X. Li, K. Wang, M. Zhong, D. Wu, H. Zhu, *Small,* 2014, **10**, 2583.
10 Z. Wen, X. Wang, S. Mao, Z. Bo, H. Kim, S. Cui, G. Lu, X. Feng, J. Chen, *Adv. Mater.,* 2012, **24**, 5610.
11 Y. Huang, J. Liang, Y. Chen, *Small,* 2012, **8**, 1805; M. F. El-Kady, R. B. Kaner, *Nat. commun.,* 2013, **4**, 1475.
12 Y. Li, Z. Li, P. Shen, *Adv. Mater.,* 2013, **25**, 2474; L. Sun, C. Tian, M. Li, X. Meng, L. Wang, R. Wang, J. Yin, H. Fu, *J. Mater. Chem. A,* 2013, **1**, 6462.
13 H. Wang, Z. Wu, F. Meng, D. Ma, X. Huang, L. Wang, X. Zhang, *ChemSusChem,* 2013, **6**, 56; Z. Wu, S. Yang, Y. Sun, K. Parvez, X. Feng, K. Mullen, *J. Am. Chem. Soc.,* 2012, **134**, 9082; Z. Wu, A. Winter, L. Chen, Y. Sun, A. Turchanin, X. Feng, K. Müllen, *Adv. Mater.,* 2012, **24**, 5130.
14 M. Zhu, X. Li, Z. Zhang, P. Sun, X. Zang, K. Wang, M. Zhong, D. Wu, H. Zhu, *Adv. Eng. Mater.* 2014, **16**, 532.
15 J. Wang, S. Kaskel, *J. Mater. Chem.,* 2012, **22**, 23710.
16 H. Deng, L. Yang, G. Tao, J. Dai, *J. Hazard. Mater.,* 2009, **166**, 1514.

17 M. Inagaki, H. Konno, O. Tanaike, *J. Power Sources,* 2010, **195**, 7880; L. Wei, G. Yushin, *Nano Energy* **2012**, *1*, 552; I. Kula, M. Uğurlu, H. Karaoğlu, A. Celik, *Bioresource Technol.,* 2008, **99**, 492.
18 N. O. Weiss, H. Zhou, L. Liao, Y. Liu, S. Jiang, Y. Huang, X. Duan, *Adv. Mater.,* 2012, **24**, 5782.
19 X. Huang, K. Qian, J. Yang, J. Zhang, L. Li , C. Yu, D. Zhao, *Adv. Mater.,* 2012, **24**, 4419; R. Mokaya, A. Pacula, *J. Phys. Chem. C,* 2008, **112**, 2764.
20 J. Schuster, G. He, B. Mandlmeier, T. Yim, K. T. Lee, T. Bein, L. F. Nazar , *Angew. Chem. Int. Ed.,* 2012, **51**, 3591; P. Lian, X. Zhu, S. Liang, Z. Li, W. Yang, H. Wang, *Electrochim. Acta,* 2010, **55**, 3909.
21 X. Huang, S. Kim, M. S. Heo, J. E. Kim, H. Suh, I. Kim, *Langmuir,* 2013, **29**, 12266.
22 J. Yan, J. Liu, Z. Fan, T. Wei, L. Zhang, *Carbon,* 2012, **50**, 2179.
23 F. Liu, S. Song, D. Xue, H. Zhang, *Adv. Mater.,* 2012, **24**, 1089.
24 R. J. J. Jansen, H. Van Bekkum, *Carbon,* 1995, **33**, 1021; Z. Li, L. Zhang, B. S. Amirkhiz, X. Tan, Z. Xu, H. Wang, B. C. Olsen, C. M. B. Holt, D. Mitlin, *Adv. Energy Mater.,* 2012, **2**, 431.
25 L. Chen, Z. Huang, H. Liang, W. Yao, Z. Yu, S. Yu, *Energy Environ. Sci.,* 2013, **6**, 3331.
26 Z. Wu, A. Winter, L. Chen, Y. Sun, A. Turchanin, X. Feng, K. Müllen, *Adv. Mater.,* 2012, **24**, 5130.
27 Y. Li, K. Sheng, W. Yuan, G. Shi, *Chem. Commun.,* 2013, **49**, 291.

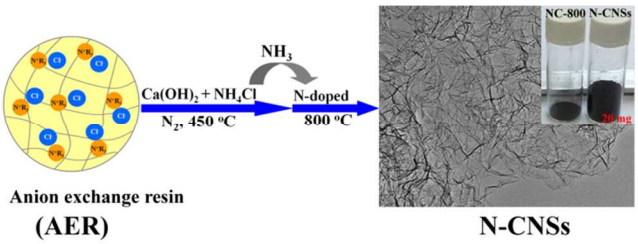

ToC Figure